Difficulties in Early Ice Detection with the Small Ice Detector-2 HIAPER (SID-2H) in Maritime Cumuli

ALEXANDRIA JOHNSON AND SONIA LASHER-TRAPP

Department of Earth, Atmospheric, and Planetary Sciences, Purdue University, West Lafayette, Indiana

AARON BANSEMER

Mesoscale and Microscale Meteorology Division, National Center for Atmospheric Research, Boulder, Colorado*

Z. ULANOWSKI

Centre for Atmospheric and Instrumentation Research, University of Hertfordshire, Hatfield, United Kingdom

ANDREW J. HEYMSFIELD

Mesoscale and Microscale Meteorology Division, National Center for Atmospheric Research, Boulder, Colorado*

(Manuscript received 29 March 2013, in final form 13 February 2014)

ABSTRACT

The Small Ice Detector, version 2 (SID-2), High-performance Instrumented Airborne Platform for Environmental Research (HIAPER; SID-2H) was used to detect small ice particles in the early stages of ice formation in the high liquid water environment of tropical maritime cumulus clouds sampled during the Ice in Clouds Experiment—Tropical (ICE-T) field campaign. Its performance in comparison to other probes and the development of new corrections applied to the data are presented. The SID-2H detected small ice crystals among larger particles. It correctly identified water drops, and discriminated between round and irregular particle shapes in water-dominated clouds with errors less than 5%. Remaining uncertainties in the sensing volume and the volume over which coincidence of particles occurred, result in the data being used here in a qualitative manner to identify the presence of ice, and its habits and sizes.

1. Introduction

The impact of ice formation on a wide range of atmospheric phenomena, from radiative transfer and precipitation to cloud lifetimes and electrification, has been well established. However, ice nucleation remains a fundamental uncertainty. In addition to the difficulty in establishing the timing and mode of ice nucleation by direct measurement, the sampling and identification of small ice particles, particularly in mixed-phase convective clouds, remains a challenge. Initial ice particles in low concentrations push the sampling volume limits of many instruments, the initial shape of ice particles may be indistinguishable from water droplets, and the resolution of most optical array probes (that have sufficient sample volumes) prevents a clear determination of the habits of particles smaller than 100 μm. As a result, our fundamental knowledge of when, where, and by what mechanisms ice first forms in convective clouds is still far from complete.

Advancements in cloud probe instrumentation have allowed the use of spatial scattering patterns, which depend on the size, shape, orientation, surface roughness, and internal structure of the particle being sampled, to aid in identifying ice. In 2001 the University of Hertfordshire developed the Small Ice Detector, version 1 (SID-1), as described by Hirst et al. (2001). It was unique, in that it had six discrete photomultiplier detectors, distributed azimuthally, allowing it to derive particle size as well as sphericity from light scattered in

*The National Center for Atmospheric Research is sponsored by the National Science Foundation.

Corresponding author address: Alexandria Johnson, Department of Earth, Atmospheric, and Planetary Sciences, Massachusetts Institute of Technology, 77 Massachusetts Ave., Cambridge, MA 02139. E-mail: avjohns@mit.edu

DOI: 10.1175/JTECH-D-13-00079.1

the forward direction. The SID-1 was used to study orographic wave clouds during the Interaction of Aerosol and Cold Clouds (INTACC) experiment (Field et al. 2001) and mixed-phase clouds (Field et al. 2004), where 1-s averages of particle properties were used to identify the dominant hydrometer phase. SID-1 was also used in the Southern African Regional Science Initiative (SAFARI 2000) field campaign to count and classify the sphericity of coarse-mode haze aerosol (Haywood et al. 2003; Osborne et al. 2004).

Improvements to SID-1 were implemented in SID, version 2 (SID-2), designed with a 24-segment azimuthal hybrid photodiode detector, allowing for the differentiation between individual supercooled liquid water and ice particles in mixed-phase clouds. Cotton et al. (2010) analyzed data from the Winter Experiments series of the Met Office (WINTEX), Cirrus and Anvils: European Satellite and Airborne Radiation (CAESAR), Geostationary Earth Radiation Budget Intercomparison of Longwave and Shortwave radiation (GERBILS), and Ice and Precipitation Initiation in Cumulus ICEPIC) field experiments. They discussed the ability of SID-2 to count, size, and determine the particle shape of sea salt and desert dust aerosols; drops in continentally influenced stratocumulus and supercooled orographic clouds; ice particles in glaciated cirrus and anvil clouds; and drops and ice in a continental mixed-phase cumulus cloud.

In 2007, the National Science Foundation (NSF) commissioned a special version of SID-2 for use with the High-performance Instrumented Airborne Platform for Environmental Research (HIAPER). The design of the SID-2 HIAPER (or SID-2H) is based on that of the SID-2 with additional improvements to its sensitivity. These include the implementation of a 100-mW laser, improved optics and a smaller beamwidth (reduced from 3 to 1.2 mm) to reduce coincidence effects, and the use of 28 azimuthally oriented detector elements, configured to detect peak signal and connected to an optical fiber relay, for capturing spatial scattering patterns.

Since the instrument's commission, it has been used in the Pacific Dust Experiment (PACDEX, 2007), the Ice in Clouds Experiment—Layer clouds (ICE-L, 2007), Stratosphere–Troposphere Analyses of Regional Transport 2008 (START08), Airborne Detector for Energetic Lighting Emission S spectra (ADELE-SPRITE, 2009), and Pre-Depression Investigation of Cloud-systems in the Tropics (PREDICT, 2010), mounted on either the NSF/National Center for Atmospheric Research (NCAR) Gulfstream V or C-130 aircraft.

However, the Ice in Clouds Experiment—Tropical (ICE-T) field campaign was the first to use SID-2H in maritime cumulus clouds, and the instrument held promise for providing the earliest detection of small ice crystals in clouds that have historically contained abundant ice at temperatures greater than −5°C (Wallace and Hobbs 2006, cf. Fig. 6.34). These clouds provided a new and challenging environment for evaluating the probe's performance and understanding its limitations, particularly in mixed-phase regions with high liquid water contents.

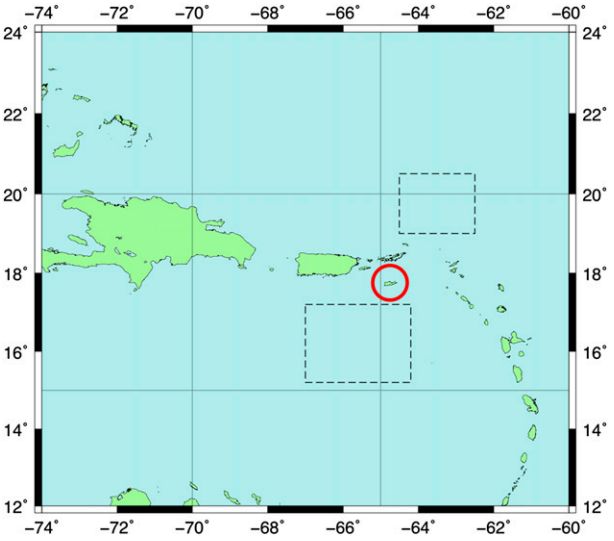

FIG. 1. Typical areas of data collection during ICE-T (boxes) within the central and eastern Caribbean. Flights were based out of St. Croix, U.S. Virgin Islands, circled in red.

The ICE-T field campaign, held in July 2011 in the central Caribbean (Fig. 1), was designed to study the mechanisms responsible and conditions required for ice nucleation, including ice nuclei measurements, in developing tropical maritime cumulus clouds. To prevent land-based aerosol contamination, the aircraft sampling avoided areas close to and immediately downwind of neighboring islands. The maritime cumulus congestus clouds targeted during ICE-T offered a simpler framework to study the production of the initial ice in cumulus clouds. Convective clouds forming over the tropical ocean are driven by surface convergence (Xue et al. 2008) in an otherwise low shear and uniform temperature environment. These localized regions of convergence result in the formation of single or successive thermals only a few kilometers wide. Such narrow clouds are thought to be the "building blocks" (Willis and Hallett 1991) of larger, multicellular storms.

The NSF/NCAR C-130 research aircraft was used as a platform for the studies conducted during ICE-T (www.eol.ucar.edu/field_projects/ice-t/). In addition to the SID-2H, the aircraft carried a scientific payload of in situ and remote sensing instruments for the measurement of background aerosols, cloud condensation and ice nuclei, cloud hydrometeors, and the cloud

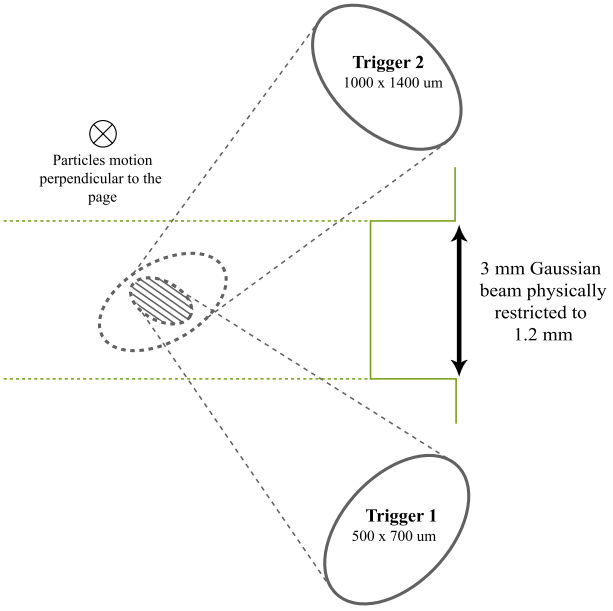

FIG. 2. Cross-section schematic of the sensing volume (shaded region) optically defined by two concentric triggers within the laser beam. (Source: adapted from University of Hertfordshire SID-2H probe overview document.)

environment. Those instruments of use for this study, in addition to the SID-2H, include the 2D Cloud (2D-C) and 2D Precipitation (2D-P) optical array probes, the Forward Scattering Spectrometer Probe (FSSP-100), 3-View Cloud Particle Imager (3V-CPI) housing a 2D Stereo (2D-S) optical array probe and a Cloud Particle Imager (CPI), and the Wyoming Cloud Radar.

In the next section, the design of SID-2H and the postprocessing software developed at NCAR are described. Initial consideration of coincidence and sample volume issues are discussed in section 3, data corrections and limitations are discussed in section 4, and section 5 illustrates the application of data corrections to several cases, including the earliest detection of small ice in ICE-T clouds. Section 6 consists of a summary and possible directions for future work.

2. SID-2H design, operation, and data processing

a. Design and operation

The SID-2H is an open path design instrument. Sampling is initiated when a particle enters the sensing volume, defined by two concentric particle detection triggers (Fig. 2), and passes through trigger 1. The particle is illuminated by a 100-mW, 532-nm Nd-YAG laser, and light scattered between 9° and 20° of the forward direction is collected by 28 azimuthally oriented detectors. The peak intensity of light incident on each detector is stored together with particle arrival time and pulse width (i.e., transit time through the laser beam). These recorded data are later fed into offline postprocessing software that sizes the particles, classifies particle shape, rejects unreliable data, and retrieves bulk properties of the particle distribution, as described in the next section.

b. Postprocessing

1) ELECTRONIC DEAD TIME

For each sampled particle, there is a 50-μs electronic dead time required for the capture and digitization of detector signals, and the transferring of the data to the computer. A simple correction for this dead time was applied by subtracting 50 μs from the sampling time, thus decreasing the sample volume, for every measured particle. Particle number concentration was then computed by dividing the number of measured particles by the adjusted sample volume. Employing this method results in number concentrations based only on the number of measured particles and the sample volume over which these particles were observed. Bulk particle concentrations are then calculated at a rate of 1 Hz. Although this method does not directly account for the number of particles passing through the sample volume during the electronic dead time,[1] it results in little to no underestimation of particle concentrations even at extremely high particle arrival rates.

2) PARTICLE SIZING

The size of particles is retrieved from the intensity of light incident on the 28 azimuthally oriented detectors and follows a power law similar to that described by Cotton et al. (2010) for SID-2:

$$r = a\overline{E}^{0.52}, \tag{1}$$

where r is the particles' derived radius, a is the power-law prefactor (a user-adjusted gain), and $\overline{E}$ represents the mean scattered light intensity recorded by the detectors after adjustment for gain and the number of light-saturated detectors. The user-adjusted gain is based on the sizing of liquid hydrometeors in warm clouds through particle size distribution and liquid water

[1] During the 50-μs electronic dead time, the SID-2H counts the number of particles passing through trigger 1 but does not record their properties (i.e., spatial scattering patterns). This "dead time count" can in principle be used to correct particle number concentrations. However, the maximum number of particles that can be counted per electronic dead time cycle is limited to 255; and in the clouds sampled during ICE-T this limit was often reached.

content comparisons between the SID-2H and the FSSP-100 or Cloud Droplet Probe (CDP). The gain is adjusted on a per-project basis and a gain value of 0.16, determined from the sampling of liquid clouds in the field, was used for the processing of ICE-T data. The exponent used here differs slightly from that presented by Cotton et al. and was derived from a fit of the Mie-scattering intensity over the angular range covered by the SID-2H detectors for particles ranging from 10 to 50 μm in diameter.

3) SHAPE DETECTION

Shape detection is accomplished following two methods. First, an asphericity factor (A_f) is computed for each particle based on the variation of scattered light intensity around the detector elements, as given by Hirst et al. (2001):

$$A_f = \frac{k}{\overline{E}} \sqrt{\sum_{i=1}^{n} (\overline{E} - E_i)^2}, \tag{2}$$

where E_i is the response of the ith detector out of the 28, $\overline{E}$ is the mean of all E_i values, and k is a scale factor such that the value of A_f is always less 100. Generally, round particles will exhibit asphericity factors between 1 and 2, while irregular particles may exhibit larger asphericity factors. Cotton et al. (2010) suggested an A_f of 6 or greater as a threshold for ice observations in the stratocumulus, mixed-phase cumulus, cirrus, and altocumulus lenticularis clouds sampled with their SID-2 probe, with further threshold refinement possible based on the size of sampled particles. However, Cotton et al. noted that the SID-2 could not discriminate the phase of all particles correctly when using only the A_f parameter in clouds with particle concentrations greater than 20 cm^{-3}.

The second method, preferred here, is to derive information on particle shape from the distribution of scattered light using a fast Fourier transform to identify strong wavenumber modes in the frequency spectrum of the azimuthal scattering patterns (Ulanowski et al. 2007, Stopford et al. 2008). Knowledge of individual ice particle habits can give insight into the nucleation temperature and/or the presence of rimed particles, and were preferred over 1-s averages of A_f, which were dominated by the water droplets in the cloud passes of interest for this study. The lack of a strong wavenumber indicates a spherical particle. Particles outside of the sampling volume typically exhibit a strong wavenumber of 1 (first harmonic) and are rejected. Particles with strong wavenumbers of 2 or 4 (second and fourth harmonic, respectively) are labeled as columns, particles with strong wavenumbers of 5 or 6 (fifth and sixth harmonic, respectively) are labeled as plates, and particles identified with the remaining wavenumber values, up to 8, are grouped into a general "irregular particle" class. This latter class may consist of complex, facetted particles; frozen droplets; or rimed ice, but they could also be prisms or rosettes with rough surfaces (Ulanowski et al. 2006, 2013; Schnaiter et al. 2011).

The identification of particle habit by the Fourier transform method was examined by plotting the percentage of particles identified as "spherical" and "nonspherical" (including column, plate, and irregular particle classes) over an entire flight and for all temperatures. The data analyzed in this way show a general separation between spherical and nonspherical particles at warm temperatures (Fig. 3), with incorrectly identified nonspheres generally below 10%, and intermixed particle types at temperatures around and below 0°C, where liquid and ice hydrometeors coexist. There is a tendency toward more nonspherical particles and fewer spherical particles at lower temperatures. A pass (Fig. 3, insert) through a glaciated cloud, as indicated by 2D-C and 2D-P images, shows that some spheres were still detected by the SID-2H, which could indicate the presence of spherical frozen drops or supercooled liquid water.

In the cloud passes of interest for this study, only a few (up to four) plates were observed. If the habit of these particles has been correctly identified by the Fourier transform, then they must have nucleated below the flight level at temperatures warmer than −4°C (because the cloud passes analyzed here were collected near cloud top) and ascended within the updraft to the temperatures at which they were sampled. The detection of so few platelike ice particles at temperatures between −3° and −7°C, and the lack of supporting plate observations on other instrumentation (2D-C, 2D-P, and 3V-CPI) suggests a false identification, unless some ice nuclei are identified, that act at such temperatures in the ICE-T environment.

4) REJECTION CRITERIA

The postprocessing software developed for the SID-2H evaluates the intensity incident on the detectors for each particle and rejects some data as unreliable. Criteria for rejection include the following:

- Nine or more azimuthal detectors have no light incident upon them
- Interarrival time less than 50 μs (the lower limit of the probe due to electronic dead time) or greater than 100 s
- Size of particle outside the expected 1–50-μm range
- Sampled particle is not symmetric about the center point of the detector, determined through the appearance of highly asymmetrical spatial scattering patterns

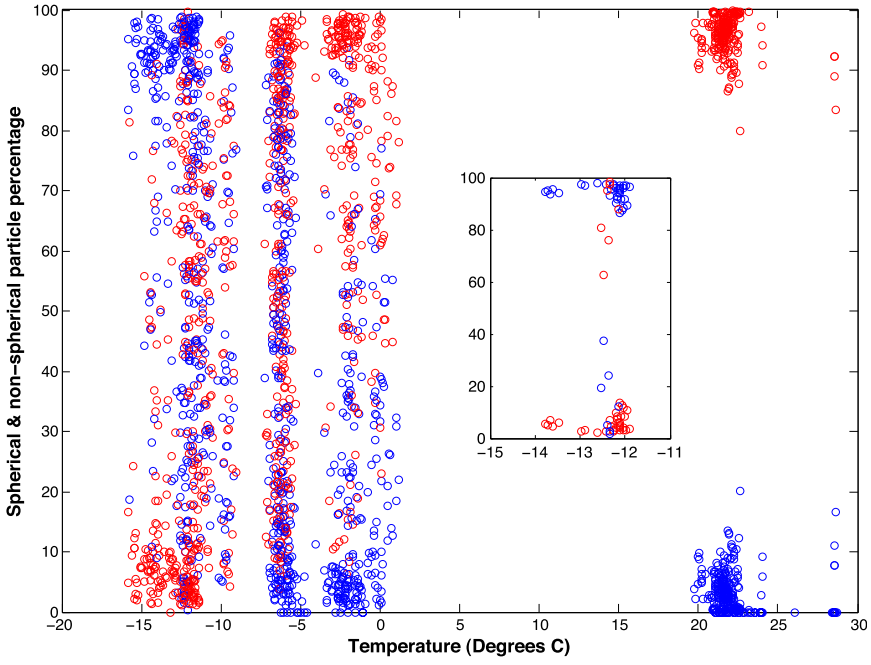

FIG. 3. SID-2H spherical (red) and nonspherical (blue; composed of column, plate, and irregular particles) observed particle percentage vs temperature for the 30 Jul 2011 research flight. (inset) A single cloud pass through a glaciated cloud, as indicated by 2D-C and 2D-P images, at −12°C.

- 10 or more detectors are saturated
- Particle transit time is less than 550 ns, the minimum transit time above the noise level of the instrument

5) BULK 1-S AND PARTICLE-BY-PARTICLE PROPERTIES

After postprocessing, the data can be viewed in terms of particle-by-particle properties, or bulk 1-s particle properties. Viewing and working with the former set of data can be labor intensive but offers insight into cloud particle variability, and allows for selective particle removal and the application of fine time-scale particle corrections. Particle-by-particle data available to the user include particle detection time, diameter, asphericity factor, particle habit derived from Fourier transform methods, transit time, (estimated) missed particle count due to the processing of the particle, mean raw scatter, rejection reason code, and the number of saturated detectors. These data are viewed using an NCAR Interactive Data Language (IDL) software package created specifically for use with the SID-2H raw data (available online from the NCAR Earth Observing Laboratory software website).

Bulk data (i.e., totals or averages over 1 s, rather than per particle) are output into a netCDF format by the IDL software and were viewed using "ncplot," a NCAR Research Aviation Facility (RAF) interactive plotting software package (available at www.eol.ucar.edu/raf/software/ncplot_dnld.html). Bulk data include accepted, rejected, and (estimated) missed particle counts; particle concentration; the percentage of particles associated with each particle habit; mean particle transit time; mean asphericity; mean particle diameter; and mean particle volume.

3. Initial analysis of SID-2H particle number concentrations

In the drop-dominated ICE-T clouds, initial comparisons between the SID-2H and the FSSP-100 were made. Both instruments detect and measure particles over the same size range (2–50 μm in diameter), have similar expected sample volumes (27.5 $cm^3 s^{-1}$ for the SID-2H and 20 $cm^3 s^{-1}$ for the FSSP-100 at airspeeds of 100 $m s^{-1}$), and use forward scattered light to sample hydrometers, but they differ in the configuration with which the scattered light is detected and how it is used in determining particle properties (Baumgardner et al. 2011). In some cloud passes, the number concentrations observed by the two instruments were nearly equal, but often the concentrations observed by the FSSP-100 were an order of magnitude or more greater than those observed by the SID-2H (Fig. 4).

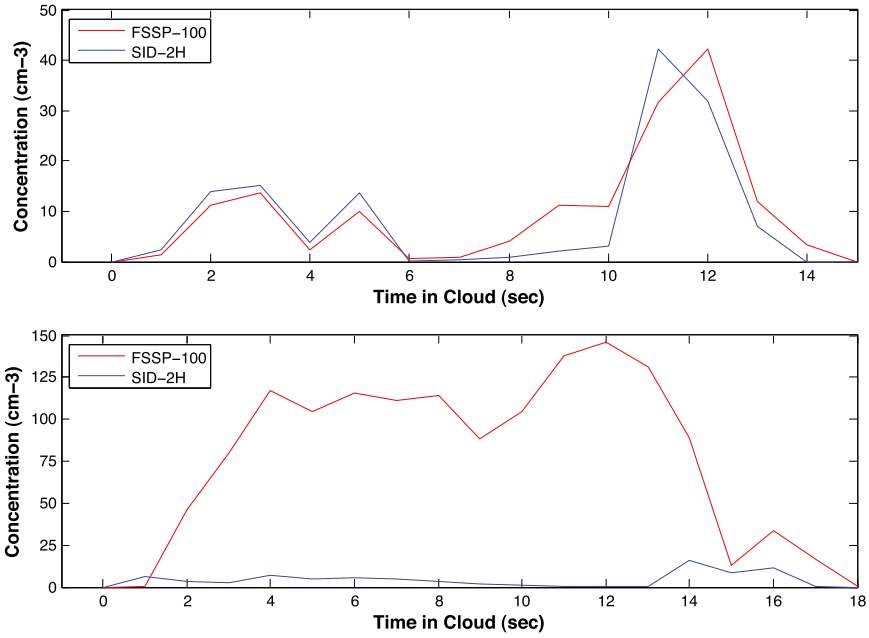

FIG. 4. (a) Cloud pass from 27 Jul 2011 (1844:49 UTC) at −13°C, where the SID-2H and FSSP-100 observed similar cloud particle concentrations. (b) Cloud pass from 11 July 2011 (1858:33 UTC) at −5°C, where the FSSP-100 observed particle concentrations are an order of magnitude or higher than the SID-2H.

It has been shown to varying degrees that the FSSP-100 suffers from drop splashing (Rogers et al. 2006) and ice particle shattering (Field et al. 2003; Korolev et al. 2011; Baumgardner et al. 2011) artifacts. Such artifacts occur when drops or large ice particles collide with the inlet shroud, subsequently break up, and shed smaller particles into the sample volume, which may artificially increase particle concentrations by orders of magnitude. Although the FSSP-100 used during ICE-T was equipped with an inlet shroud, the cases of interest here were water dominated, containing very few ice particles, and the degree to which the in situ observations suffer from shattering and splashing artifacts has yet to be determined. However, these artifacts may be, in part, responsible for the discrepancy between SID-2H and FSSP-100 particle concentrations.[2]

Errors in the concentration of particles observed by SID-2H may arise due to coincidence effects. These effects are the result of multiple particles in the sensing volume, either at one instance or over some time, when a single instance of instrument sampling has been initiated. Particle coincidence in optical particle counters like the FSSP-100 has been studied extensively (e.g., Baumgardner et al. 1985; Brenguier et al. 1994), and the analysis that follows is based on similar principles. These studies also outlined two types of information loss due to coincidence: retriggerable delay losses, discussed below; and sampled particle coincidence losses, addressed in section 4a.

Retriggerable delay losses arise from a "string" of particles entering trigger 1 shortly after one another and before the previous particle (or particles) has left. In this instance the string of particles may be detected as a single particle, resulting in an underestimate of concentrations and longer-than-expected dead times known as a "retriggerable delay" (Baumgardner et al. 1985). Evidence of retriggerable delay losses on the SID-2H data was sought by plotting high-rate (10 Hz) FSSP-100 concentrations versus the SID-2H particle interarrival times over the same period. When the FSSP-100 particle number concentrations increased above 60 cm^{-3}, the minimum SID-2H-observed interarrival times was also, unexpectedly, found to increase. This trend was observed in six cloud passes, through clouds in their

[2] The CDP, which has no shroud and would produce less splashing and shattering artifacts, collected data during ICE-T for the first five flights (1, 4, 6, 11, and 12 July 2011). On the 12 July flight, the CDP was damaged by a static discharge and replaced with a second CDP of undetermined sample volume. Comparisons between SID-2H and CDP number concentrations from the first several flights showed similar trends to the SID-2H and FSSP-100 comparison, with the CDP tending to match the SID-2H data better overall in these limited comparisons. However, the cases of interest for this study occurred later in the project, when the CDP data were not available.

early ice formation stages, from four separate research flights. Theoretically a clustering of particle interarrival times near the minimum 50-μs limit [due to the electronic dead time discussed in section 2b(1)] would be expected with increasing particle concentration, but this was not observed and retriggerable delay losses are suspected as the cause.[3]

Estimates of the degree to which retriggerable delay losses may be affecting SID-2H interarrival times and particle concentrations were made assuming all particles were 50 μm in diameter, distributed equally in space, and passed through the depth of the SID-2H sensing volume (210 μm) at an airspeed of 130 m s^{-1}. From these assumptions, particles must arrive within 2 μs of one another for a loss to be observed. A Poisson distribution of interarrival times was then used to predict the percentage of particles with interarrival times less than 2 μs, and ranged from 2.9×10^{-5}% at 50 cm^{-3} to 1.4×10^{-3}% at 100 cm^{-3}. Additionally, it is not until particle number concentrations exceed 91 cm^{-3} over an entire second that two particles would begin arriving within 2 μs of each other. These estimates indicate that retriggerable delay losses should not be observed until concentrations of 90 cm^{-3} are reached; yet SID-2H particle interarrival times begin increasing at FSSP-100 concentrations as low as 50 cm^{-3}. Thus, it is possible that this loss can explain some, but not all, of the observed data anomalies in particle number concentration measured by the SID-2H during the ICE-T field campaign.

In addition, it is likely that errors in the particle concentrations from the SID-2H arise from uncertainties in the volume over which the instrument suffers from coincidence effects. An estimated extended sensing volume of 12 mm^3, including a volume outside and within trigger 1, was calculated based on SID-2 optical system modeling. NCAR's modifications to the SID-2H reduced this extended volume by reducing the beamwidth, but similar optical modeling studies have not yet been performed.

Testing of the volume of coincidence for SID-2H in the laboratory is planned (J. Stith 2013, personal communication), but such procedures are not as straightforward as the testing of other probes, like the CDP, with droplet generators (Lance et al. 2010). The SID-2H relies on two-dimensional scattering patterns, and the optics must be able to view a much larger volume than trigger 1. The ability to sense particles in this extended volume leads to increased coincidence effects at high particle concentrations.

Despite these remaining issues, partial corrections were developed and applied to the SID-2H data, which, in conjunction with data from imaging probes, can provide some limited information on the presence of small ice particles in mixed-phase clouds. The next section discusses these corrections in detail.

4. Correction methods

a. Sampled particle coincidence loss

As discussed in the last section, the presence of two or more particles in the extended sensing volume at one instance, leading to sampled particle coincidence losses, can result in an underestimation of particle concentrations and subsequent false identification of particle habits by the SID-2H.

When sampling is initiated by a particle passing through trigger 1 and more than one particle is within the extended sensing volume of the instrument, their combined scattering pattern is likely to be interpreted as that of a single, irregular particle. One way to address this problem is through the use of Poisson statistics, which assumes that the sampling of the hydrometeor population resembles a Poisson process, where sampled particles are assumed to be statistically uniform and independently distributed in space (Kostinski and Shaw 2001). From this the probability of x particles in the extended sensing volume can be calculated [Eq. (3.1)] if the mean number of particles in the volume is given by λ, which depends on the total concentration of particles less than 50 μm observed in the cloud N; the cross-sectional area of extended sensing volume perpendicular to the direction of flight A; and the depth of the beam d [Eq. (3.2)].

To estimate the effects of coincidence as realistically as possible, the probability of coincidence was calculated using the total number concentration of particles less than 50 μm observed by the FSSP-100. Often this instrument observed concentrations within the expected range for maritime environments; however, there may have been instances when the FSSP-100 concentration was artificially increased by drop splashing or ice shattering on the inlet shroud. When the correction method outlined in this section is applied using the FSSP-100 number concentration, and if it is artificially increased by these means, a greater number of irregular particles will be removed, resulting in a more drastic correction. The preference in this study was that the ice particle counts should be underestimated rather than overestimated.

[3] One would also expect longer interarrival times with decreasing particle number concentrations to be evident but that was not observed. The independence between SID-2H interarrival times and FSSP-100 concentrations might be explained by particle clustering at low concentrations, but a thorough investigation requires additional information that was not collected during ICE-T.

Ideally, one would develop a correction scheme based upon the SID-2H data alone, but a suitable algorithm has not yet been found.

Using this information the probability of two or more particles in this volume at one time can then be calculated [Eq. (3.3)] and the probable fraction of falsely identified irregular particles derived:

$$P(x,\lambda) = \frac{\lambda^x \exp(-\lambda)}{x!} \tag{3.1}$$

$$\lambda = NAd \tag{3.2}$$

$$P(x>1,\lambda) = 1 - \exp(-\lambda)(1+\lambda). \tag{3.3}$$

The observed number of irregular particles is then corrected by subtracting the derived fraction of falsely identified irregular particles. Because in the early ice formation stage, which is of interest in this study, drops greatly outnumber ice particles, it can then be inferred that the majority of coincidence effects occur from the presence of multiple drops in the sensing volume at one time. Thus, the number of spheres detected by SID-2H was corrected by adding back twice the number of particles removed from the irregular particle category, as this is the number of particles most likely to be coincident within the extended sensing volume at any given time.

The extended sensing volume for the SID-2H is not clearly defined, however. Optimally, coincidence would be observed only if particles were collocated in the area of trigger 1 (Fig. 2) through which a particle must pass in order to initiate sampling. In practice, this area includes trigger 2 and may extend beyond into the total cross-sectional area of the beam (1.2 mm × 8 mm). In the calculation of coincidence outlined above, an area equal to that of trigger 2 has been assumed, equivalent to 0.011 cm^2, a conservative estimate that will lead to removal of some but not all irregular particles. The depth of the beam is known to be 210 μm, resulting in an extended sensing volume of 0.0023 cm^3. Using this information and Eq. (3.3), the largest probability of coincidence is associated with the presence of two particles in the extended sensing volume for the typical particle concentrations observed during ICE-T (probabilities of 0.001%–0.224% for concentrations of 20–300 cm^{-3} respectively). If coincidence were to be calculated using the entire cross section of the beam, then the probability of two or more particles in the sensing volume would increase to 0.079% and 12.3% for concentrations of 20 and 300 cm^{-3}, respectively. Applying such corrections to the data would remove most or all of the irregular particles observed by SID-2H, some of which are likely present in the clouds at temperatures less than 0°C.

b. Repeating patterns

Another correction to the SID-2H data was the removal of particles near the minimum detectable size limit of the instrument. Operationally this size is 1 μm, and particles that fall close to this limit tend to produce repeating scattering patterns that are dominated by the noise of the instrument (Fig. 5). Currently, the identification of these repeated patterns is a manual process that involves viewing and inspecting the mean raw scatter of a sample population of 100 particles for each second of a cloud pass as shown. Because the size of a particle is directly related to its mean raw scatter value, noise-dominated patterns are often observed in the 0–200 mean raw scatter range, which corresponds to particles sizes of 1.0–10.5 μm. Once particles with repeated patterns are visually identified in the mean raw scatterplots, the diameter and strong wavenumber of these particles (the number before and after the decimal, respectively, noted next to each particle in Fig. 5) are used to selectively remove all particles with matching characteristics. The identification and removal of these particles in the particle-by-particle files is performed manually with a matrix laboratory (MATLAB) program for that second of flight and, if desired, 1-s bulk particle properties can be recalculated. Particles removed by this correction were all identified as columns or irregular particles with typical diameters of 5 μm or less.

5. Results and comparisons with other data

With the application of these corrections, greater confidence is placed on the detection of spheres, columns, and irregular particles by the SID-2H in cold clouds. These corrections are not successful in resolving the discrepancies between the FSSP-100 and corrected SID-2H total particle concentrations. Thus, the following analysis focuses on the number of particles (particle counts) of each habit observed by SID-2H, rather than the number concentration of particles, as a means of investigating what information can be gained from the SID-2H data regarding small ice particles in the maritime cumuli sampled during the ICE-T field campaign. Comparisons to other probes are also conducted: a 3V-CPI, housing a 2D-S probe and a CPI, capable of viewing particles from 10–1260 μm and >3 μm, respectively (Baumgardner et al. 2011), was also flown during ICE-T, as were 2D-C and 2D-P optical array probes.

a. Warm cases

Cloud passes at temperatures well above 0°C were sometimes performed during ICE-T to document the productivity of the warm rain process and to sample characteristics at the warm cloud bases. These passes

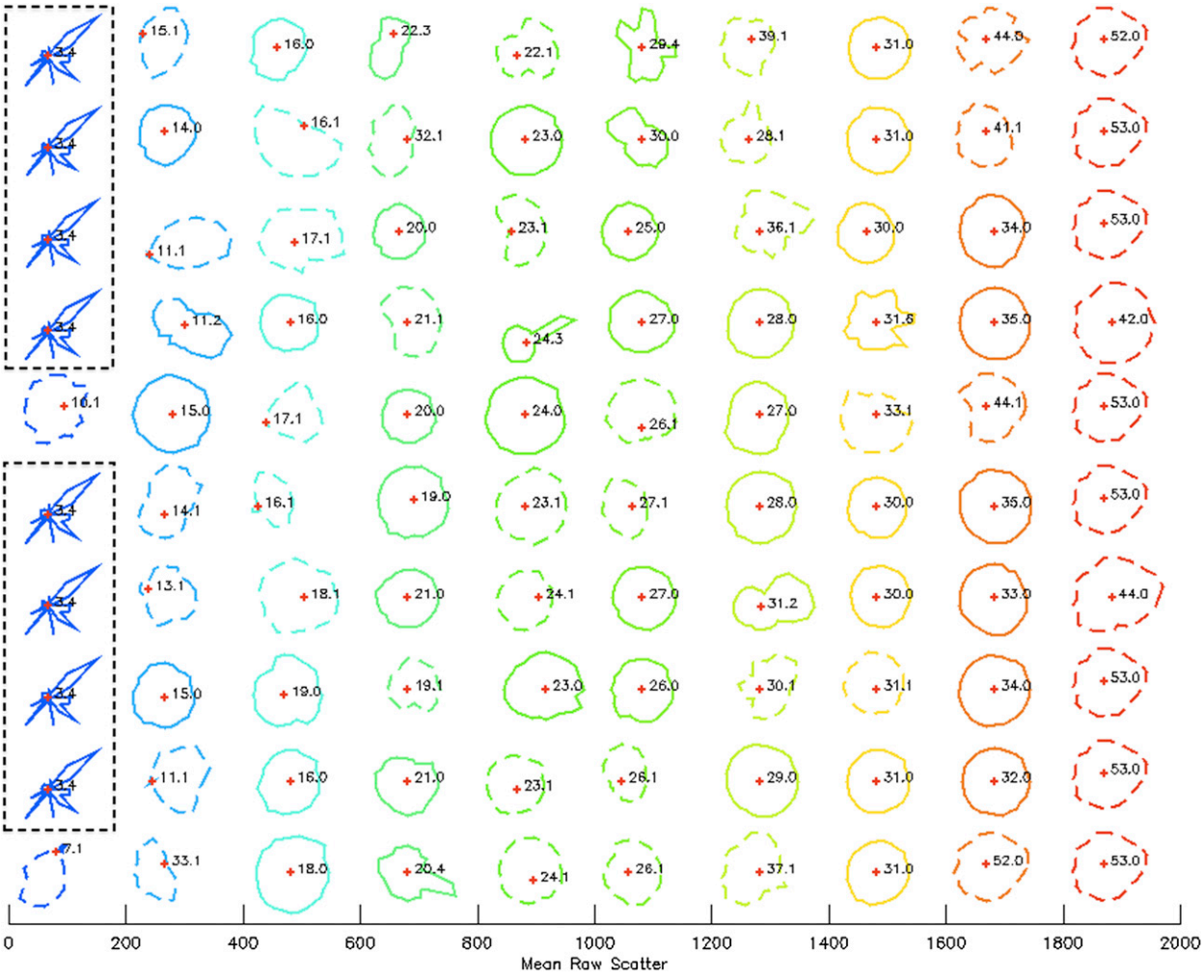

FIG. 5. Mean raw scatterplots for 1-s of flight (1818:50 UTC 12 Jul 2011) through a cloud as viewed in the SID-2H IDL postprocessing software. The eight particles in dashed rectangles on the left represent particles with a repeating scattering pattern. The number before the decimal next to each particle represents its estimated size (in μm) and the number after the decimal represents the strongest wavenumber associated with the scattering pattern. Particle color is respective of the mean raw scatter bin in which the particle is assigned; solid outlines represent accepted and dashed lines represent rejected particles by the software as described in section 2b(4).

also provided an opportunity to investigate the SID-2H instrument response in the absence of ice. In Fig. 6 two different occurrences of warm cloud passes through growing cumulus congestus near cloud top, where only liquid (spherical) drops would occur, are shown. The corrections discussed in the previous section have been applied to the data, as indicated by the change between the dashed and solid lines.

In the first example (Fig. 6, top panel), irregular particles were rarely detected, and the correction algorithms removed almost all such particles. A few irregular particles remain between 8 and 11 s, comprising at most 5% of the total particle count. These particles are suspected to be from additional particle coincidence effects. In the second example (Fig. 6, bottom panel), irregular particles were observed at 2 s into the cloud pass, all of which were removed by the application of the corrections described in section 4.

In both of these cases, no ice was detected by the 2D-C, 2D-P, 2D-S, or CPI probes. It is clear from these plots that the majority of particles are correctly identified as spherical water drops by the SID-2H, with a false detection rate for irregular particles being as much as 7% before corrections but decreasing to less than 5% after the corrections. As also shown in Fig. 3 and discussed in section 2b(3), the SID-2H probe discriminates between round and irregular particle shapes in a number of warm, water-dominated clouds with little error (<5%).

b. *Early ice cases*

Following the laboratory studies by Kaye et al. (2008) and Ulanowski et al. (2006), who demonstrated that

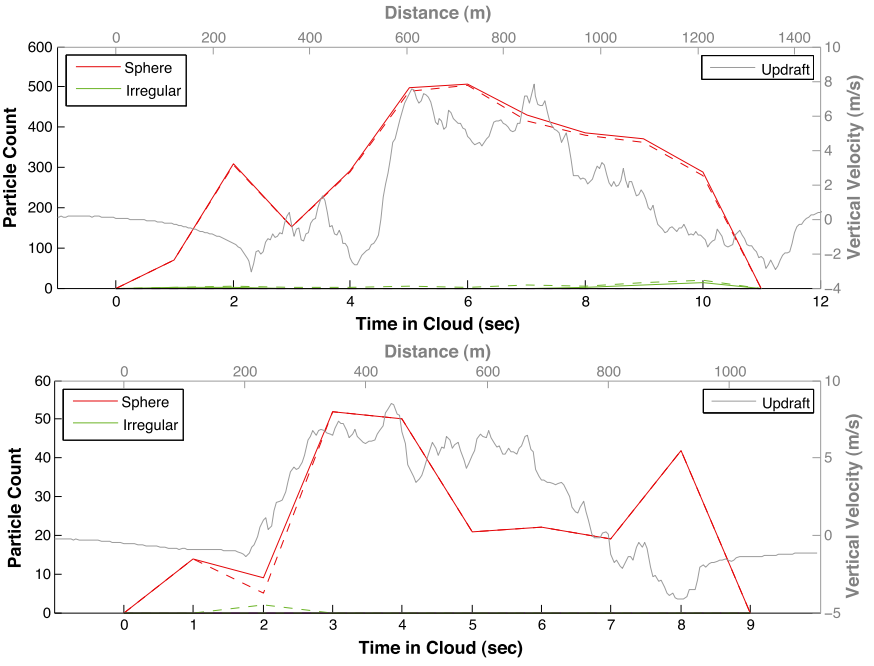

FIG. 6. Warm cloud passes at +7°C from (a) 11 Jul 2011, starting at 1810:49 UTC; and (b) 12 Jul 2011, starting at 1844:33 UTC, within 500 m of the cloud top. Original (dashed lines) and corrected (solid lines) particle counts for sphere and irregular particles detected by the SID-2H (left axis) and updraft vertical velocity (gray line, right axis) as measured during the cloud pass over time (bottom axis) and distance in cloud (top axis).

clear habit scattering patterns originate from pristine ice particles, any particles identified as columns that remain after the removal of repeated scattering patterns are assumed to be real and relatively pristine. The true morphology of particles placed in the ''irregular'' particle class is unknown, but may it include rimed frozen drops and rimed ice crystals, frozen raindrop fragments (Rangno and Hobbs 2005), and rough-facetted particles, including prisms (Ulanowski et al. 2006, 2013).

Two examples of cases where the SID-2H detected ice in cloud passes with temperatures less than 0°C are now presented. These cases were selected because the cloud passes were within 500 m of cloud top (as shown by the Wyoming Cloud Radar) in clouds with vigorous updrafts, and are of interest for investigating how early the SID-2H can detect ice.

In the first example (Fig. 7), the cloud temperature ranged from −6° to −7°C. The application of coincidence corrections decreased the irregular particles slightly between 4 and 7 s into the cloud pass, and the removal of repeated scattering patterns decreased the number of columns observed 8 s into the cloud. A peak in the overall number of ice particles is observed at this time, collocated with the edge of the updraft. The mean column and irregular diameters at this time are 4 μm. Larger graupel (up to 3 mm) and columns (up to 91 μm) were detected by the 2D-C probe (red images) and 2D-S probe (blue images) during the times that the SID-2H recorded these particles, corroborating the presence of ice.

In the second example (Fig. 8), the cloud temperature ranged from −5° to −6°C. Here, too, the coincidence corrections made small decreases in the number of irregular particles (most easily seen by the increase in spheres from 2 to 4 s into the cloud pass), and reductions in columns and irregular particles owing to the removal of repeated scattering patterns occurred from 3 to 7 s. The 2D-S images show the presence of graupel and columns during this time as well. The majority of the ice was again found at the edge of the updraft (mean column diameter of 4 μm and mean irregular diameter of 9 μm) or within the updraft/downdraft interface (mean column diameter of 7 μm and mean irregular diameter of 13 μm), but a few columns and irregular particles were detected in the main updraft (4 s into the cloud pass, mean irregular diameter of 10 μm). During this cloud pass, the 2D-C probe recorded no images of ice particles, but the upper size limit of ice particles detected by the SID-2H is 50 μm, essentially undetectable by the 2D-C probe.

In both of these cloud passes, and in others occurring in similar environments during the ICE-T field campaign,

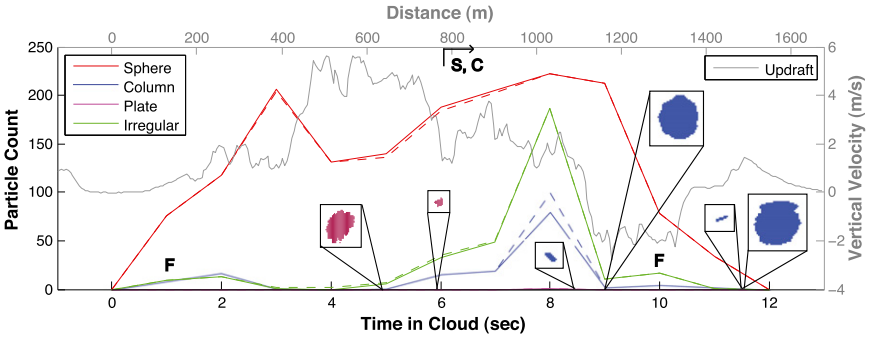

FIG. 7. As in Fig. 6, but early ice case from 12 Jul 2011 starting at 1818:43 UTC and with column and plate particles also. Sample particle images from the 2D-C (pink) and 2D-S (blue) with their location are shown. Symbols: F represents the start and end of the cloud pass as observed by the FSSP-100 (concentrations $> 1\ \mathrm{cm}^{-3}$); S and C indicate the time at which data from the 2D-S and CPI, respectively, became available.

the SID-2H detected columns and irregular particles with sizes as small as a few microns in diameter, in the presence of graupel and larger columns detected by some of the optical array probes. Additionally, the percentage of irregular particles in these cases often exceeds the percentage of falsely identified irregular particles in warm cloud passes (i.e., >5%), a further indication that a small ice population may coexist with larger ice particles in these clouds.

The appearance of the first detectable ice, albeit at larger sizes, near the cloud edge in downdrafts has also been observed in past studies (e.g., Young 1974; Blyth and Latham 1993). The SID-2H data may thus be useful in identifying ice particles at an earlier stage of their growth, where their locations could be linked to primary nucleation processes or secondary processes, such as rime-splintering (Hallett and Mossop 1974), in the cases shown.

6. Summary and future work

ICE-T was the first field campaign to use SID-2H for the detection of small ice particles in tropical maritime cumulus clouds that contained an abundance of liquid water, and initially very few ice particles. Analysis of these SID-2H data have allowed for a better understanding of the probe response to the detection of ice under such conditions.

Corrections to the data have been developed and applied here. They include an algorithm to adjust for particle coincidence, based on an independent estimate of the droplet number concentration detected by the FSSP-100, and an algorithm for the manual removal of repeated scattering patterns, when particles near the minimum detectable size of the instrument are sampled. With the application of these corrections, the number of spheres, columns, and irregular particles detected by SID-2H were used to inspect the small hydrometeor population of a cloud.

In warm cloud test cases, SID-2H correctly identified water drops, and in water-dominated clouds it discriminated between round and irregular particle shapes with errors less than 5% in the worst cases. In terms of ice detection in the presence of liquid water, the false-positive rate may partly be a consequence of

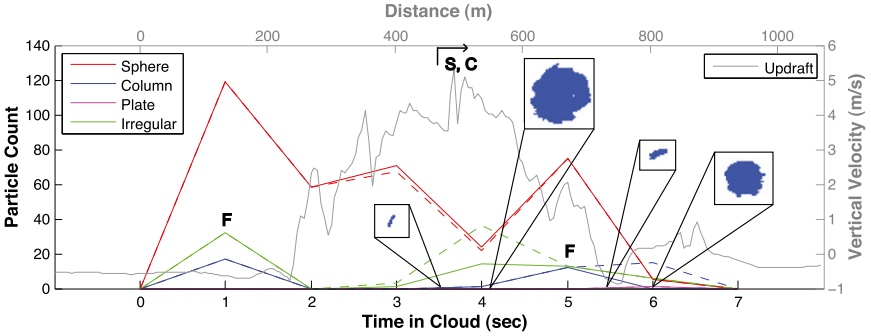

FIG. 8. As in Fig. 7, but from 30 Jul 2011, starting at 1627:25 UTC. No 2D-C images of ice were found during this cloud pass.

the dominant presence in many cloud types of highly irregular or rough ice particles (Ulanowski et al. 2013; Cole et al. 2013; Baran 2012), which produce azimuthally symmetric scattering patterns. In such cases the higher-resolution Small Ice Detector, version 3 (SID-3), probes may offer better shape discrimination capability (Ulanowski et al. 2006, 2013; Kaye et al. 2008).

In the examples of interest here, where the first detectable ice was sought near cloud top in the developing cumuli, the SID-2H identified smaller ice crystals (columns and irregular, perhaps rimed ice, particles) among larger columns and graupel within the temperature range known to accommodate the rime-splintering mechanism. Future work will include numerical modeling of this process to investigate the importance of this possible ice multiplication mechanism early on in the ICE-T clouds.

This study has also identified some troubling problems with the SID-2H probe that prevent accurate quantification of particle number concentrations in particle-dense clouds. Uncertainties in the sampling volume, including that over which coincidence may occur, remain. An evaluation of this volume may require a mapping of the laser beam dimensions, modeling of the optical system, and testing the volume along the beam over which coincident particles would lead to combined scattering patterns. Comparison studies between the FSSP-100, CDP, and SID-2H (including but not limited to interarrival time analysis and shattering studies) with the instruments in close proximity to one another are recommended in future campaigns and may shed light on concentration discrepancies between the FSSP-100 and SID-2H observed in the ICE-T data.

The loss of particle information due to retriggerable delays and coincidence prevents meaningful estimates of particle number concentrations when the droplet number density is high, such as in water-dominated mixed-phase clouds observed during ICE-T. This limitation suggests that the SID-2H can only be used to discriminate particle habit in such clouds (after the application of coincidence corrections presented here), and that the quantification of new ice particles in this environment is still elusive.

Future investigation of the particle scattering patterns with the use of Monte Carlo simulations could aid in determining how coincident particles of a particular habit are classified. Such work would expand our knowledge of the instruments' response to coincidence, and the resulting particle shape interpretation, which appears to be the main utility of this probe, at this time, in water-dominated mixed-phase clouds.

Acknowledgments. Our gratitude is expressed to all of the participants of ICE-T for their roles in the data collection effort, and especially the Research Air Facility (RAF) at NCAR and the University of Wyoming's Department of Atmospheric Science for their data processing and analysis software. The authors also thank Paul Kaye and Edwin Hirst, at the University of Hertfordshire's Centre for Atmospheric and Instrumentation Research (CAIR), for their work developing and building the SID-2H; Dave Rogers and Jeff Stith of NCAR RAF for their helpful suggestions and conversations; and D. Baumgardner and an anonymous reviewer for their help in improving the manuscript substantially. This study was funded by NSF Award AGS-1032972.

REFERENCES

Baran, A. J., 2012: From the single-scattering properties of ice crystals to climate prediction: A way forward. *Atmos. Res.,* **112,** 45–69, doi:10.1016/j.atmosres.2012.04.010.

Baumgardner, D., W. A. Cooper, and J. E. Dye, 1985: Evaluation of the Forward Scattering Spectrometer Probe. Part II: Corrections for coincidence and dead-time losses. *J. Atmos. Oceanic Technol.,* **2,** 626–632, doi:10.1175/1520-0426(1985)002<0626:EOTFSS>2.0.CO;2.

——, and Coauthors, 2011: Airborne instruments to measure atmospheric aerosol particles, clouds and radiation: A cook's tour of mature and emerging technology. *Atmos. Res.,* **102,** 10–29, doi:10.1016/j.atmosres.2011.06.021.

Blyth, A. M., and J. Latham, 1993: Development of ice and precipitation in New Mexican summertime cumulus clouds. *Quart. J. Roy. Meteor. Soc.,* **119,** 91–120, doi:10.1002/qj.49711950905.

Brenguier, J. L., D. Baumgardner, and B. Baker, 1994: A review and discussion of processing algorithms for FSSP concentration measurements. *J. Atmos. Oceanic Technol.,* **11,** 1409–1414, doi:10.1175/1520-0426(1994)011<1409:ARADOP>2.0.CO;2.

Cole, B. H., P. Yang, B. A. Baum, J. Riedi, L. C.-Labonnote, F. Thieuleux, and S. Platnick, 2013: Comparison of PARASOL observations with polarized reflectances simulated using different ice habit mixtures. *J. Appl. Meteor. Climatol.,* **52,** 186–196, doi:10.1175/JAMC-D-12-097.1.

Cotton, R., S. Osborne, Z. Ulanowski, P. H. Kaye, and R. S. Greenaway, 2010: The ability of the Small Ice Detector (SID-2) to characterize cloud particle and aerosol morphologies obtains during flights of the FAAM BAe-146 research aircraft. *J. Atmos. Oceanic Technol.,* **27,** 290–303, doi:10.1175/2009JTECHA1282.1.

Field, P. R., and Coauthors, 2001: Ice nucleation in orographic wave clouds: Measurements made during INTACC. *Quart. J. Roy. Meteor. Soc.,* **127,** 1493–1512, doi:10.1002/qj.49712757502.

——, R. Wood, P. R. A. Brown, P. H. Kaye, E. Hirst, R. Greenway, and J. A. Smith, 2003: Ice particle interarrival times measured with a fast FSSP. *J. Atmos. Oceanic Technol.,* **20,** 249–261, doi:10.1175/1520-0426(2003)020<0249:IPITMW>2.0.CO;2.

——, R. J. Hogan, P. R. A. Brown, A. J. Illingworth, T. W. Choularton, P. H. Kaye, E. Hirst, and R. Greenway, 2004: Simultaneous radar and aircraft observations of mixed-phase clouds at 100 m scale. *Quart. J. Roy. Meteor. Soc.,* **130,** 1877–1904, doi:10.1256/qj.03.102.

Hallett, J., and S. C. Mossop, 1974: Production of secondary ice particles during the riming process. *Nature,* **249,** 26–28, doi:10.1038/249026a0.

Haywood, J. M., S. R. Osborne, P. N. Francis, A. Keil, P. Formenti, M. O. Andreae, and P. H. Kaye, 2003: The mean physical and optical properties of regional haze dominated by biomass burning aerosol measured from the C-130 aircraft during SAFARI 2000. *J. Geophys. Res.,* **108,** 8473, doi:10.1029/2002JD002226.

Hirst, E., P. H. Kaye, R. S. Greenaway, P. Field, and D. W. Johnson, 2001: Discrimination of micrometre-sized ice and super-cooled droplets in mixed-phase cloud. *Atmos. Environ.,* **35,** 33–47, doi:10.1016/S1352-2310(00)00377-0.

Kaye, P. H., E. Hirst, R. S. Greenway, Z. Ulanowski, E. Hesse, P. J. DeMott, C. Saunders, and P. Connolly, 2008: Classifying atmospheric ice crystals by spatial light scattering. *Opt. Lett.,* **33,** 1545–1547, doi:10.1364/OL.33.001545.

Korolev, A. V., E. F. Emery, J. W. Strapp, S. G. Cober, G. A. Isaac, M. Wasey, and D. Marcotte, 2011: Small ice particles in tropospheric clouds: Fact or artifact? Airborne Icing Instrumentation Evaluation Experiment. *Bull. Amer. Meteor. Soc.,* **92,** 967–973, doi:10.1175/2010BAMS3141.1.

Kostinski, A. B., and R. A. Shaw, 2001: Scale-dependent droplet clustering in turbulent clouds. *J. Fluid Mech.,* **434,** 389–398, doi:10.1017/S0022112001004001.

Lance, S., C. A. Brock, D. Rogers, and J. A. Gordon, 2010: Water droplet calibration of the Cloud Droplet Probe (CDP) and in-flight performance in liquid, ice and mixed-phase clouds during ARCPAC. *Atmos. Meas. Tech.,* **3,** 1683–1706, doi:10.5194/amt-3-1683-2010.

Osborne, S. R., J. M. Haywood, P. N. Francis, and O. Dubovik, 2004: Short-wave radiative effects of biomass burning aerosol during SAFARI 2000. *Quart. J. Roy. Meteor. Soc.,* **130,** 1423–1447, doi:10.1256/qj.03.134.

Rangno, A. L., and P. V. Hobbs, 2005: Microstructures and precipitation development in cumulus and small cumulonimbus clouds over the warm pool of the tropical Pacific Ocean. *Quart. J. Roy. Meteor. Soc.,* **131,** 639–673, doi:10.1256/qj.04.13.

Rogers, D. C., J. Stith, J. Jensen, W. A. Cooper, D. Nagel, U. Maixner, and O. Goyea, 2006: Splash artifacts in FSSP measurements—Observations and flow modeling studies. Preprints, *12th Conf. on Cloud Physics,* Madison, WI, Amer. Meteor. Soc., P2.30. [Available online at https://ams.confex.com/ams/Madison2006/techprogram/paper_112416.htm.]

Schnaiter, M., P. H. Kaye, E. Hirst, Z. Ulanowski, and R. Wagner, 2011: Exploring the surface roughness of small ice crystals by measuring high resolution angular scattering patterns. *Atti Accad. Peloritana Pericolanti, Cl. Sci. Fis., Mat. Nat.,* **89** (Suppl.), doi:10.1478/C1V89S1P084.

Stopford, C., Z. Ulanowski, E. Hesse, P. H. Kaye, E. Hirst, M. Schnaiter, and D. McCall, 2008: Initial investigation into using Fourier spectra as a means of classifying ice crystal shapes. *Proceedings of the 11th Conference on Electromagnetic and Light Scattering,* University of Hertfordshire, 247–250.

Ulanowski, Z., E. Hesse, P. H. Kaye, and A. J. Baran, 2006: Light scattering by complex ice-analogue crystals. *J. Quant. Spectrosc. Radiat. Transfer,* **100,** 382–392, doi:10.1016/j.jqsrt.2005.11.052.

——, C. Stopford, E. Hesse, P. H. Kaye, E. Hirst, and M. Schnaiter, 2007: Characterization of small ice crystals using frequency analysis of azimuthal scattering patterns. *Peer-Reviewed Abstracts of the Tenth Conference on Electromagnetic and Light Scattering,* G. Videen et al. Eds., ICHMT, 225–228.

——, P. H. Kaye, E. Hirst, R. S. Greenaway, R. J. Cotton, E. Hesse, and C. T. Collier, 2013: Incidence of rough and irregular atmospheric ice particles from Small Ice Detector 3 measurements. *Atmos. Chem. Phys. Discuss.,* **13,** 24 975–25 012, doi:10.5194/acpd-13-24975-2013.

Wallace, J. M., and P. V. Hobbs, 2006: *Atmospheric Science: An Introductory Survey.* International Geophysics Series, Vol. 92, Academic Press, 483 pp.

Willis, P. T., and J. Hallett, 1991: Microphysical measurements from an aircraft ascending with a growing isolated maritime cumulus tower. *J. Atmos. Sci.,* **48,** 283–300, doi:10.1175/1520-0469(1991)048<0283:MMFAAA>2.0.CO;2.

Xue, H., G. Feingold, and B. Stevens, 2008: Aerosol effects on clouds, precipitation, and the organization of shallow cumulus convection. *J. Atmos. Sci.,* **65,** 392–406, doi:10.1175/2007JAS2428.1.

Young, K. C., 1974: The role of contact nucleation in ice phase initiation in clouds. *J. Atmos. Sci.,* **31,** 768–776, doi:10.1175/1520-0469(1974)031<0768:TROCNI>2.0.CO;2.